Exceptional Charge Transport Properties of Graphene on Germanium

Francesca Cavallo,[*,∥,†,§] Richard Rojas Delgado,[∥,†] Michelle M. Kelly,[‡,⊥] José R. Sánchez Pérez,[†] Daniel P. Schroeder,[†] Huili Grace Xing,[‡] Mark A. Eriksson,[†] and Max G. Lagally[*,†]

[†]University of Wisconsin-Madison, Madison, Wisconsin 53706, United States, and [‡]University of Notre Dame, Notre Dame, Indiana 46556, United States. [∥]F. Cavallo and R. Rojas Delgado contributed equally to the work. [§]Present address: University of New Mexico, Albuquerque, New Mexico 87106, United States. [⊥]Present address: 6537 Aylesboro Avenue, Pittsburgh, Pennsylvania 15217, United States.

ABSTRACT The excellent charge transport properties of graphene suggest a wide range of application in analog electronics. While most practical devices will require that graphene be bonded to a substrate, such bonding generally degrades these transport properties. In contrast, when graphene is transferred to Ge(001) its conductivity is extremely high and the charge carrier mobility derived from the relevant transport measurements is, under some circumstances, higher than that of freestanding, edge-supported graphene. We measure a mobility of $\sim 5 \times 10^5$ cm^2 V^{-1} s^{-1} at 20 K, and $\sim 10^3$ cm^2 V^{-1} s^{-1} at 300 K. These values are close to the theoretical limit for doped graphene. Carrier densities in the graphene are as high as 10^{14} cm^{-2} at 300 K.

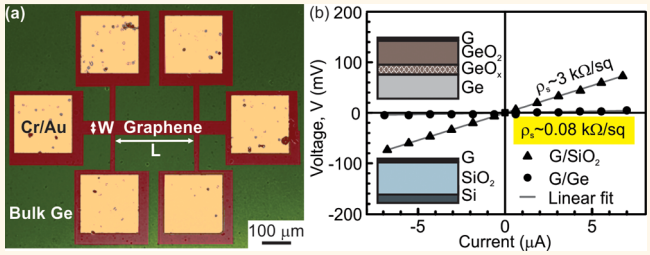

KEYWORDS: graphene · Germanium substrate · interface states · doping · high mobility · low sheet resistivity

Exfoliated monolayer graphene suspended and contacted at its ends exhibits mobility values of $\sim 10^5$ cm^2 V^{-1} s^{-1} at temperatures between 5 to 240 K, with carrier concentrations $n_G \sim 10^{11}$–10^{12} cm^{-2}.[1−3] Corresponding resistivity values are of the order of $\rho \sim 1$–$10\ \mu\Omega$ cm, *i.e.*, comparable to the resistivity of Cu ($\rho \sim 0.6\ \mu\Omega$ cm) and lower than the resistivity of indium tin oxide (ITO) ($\rho \sim 620\ \mu\Omega$ cm).[4] Furthermore, the thermal conductivity of graphene has been measured to be approximately ~ 5000 Wm^{-1} K^{-1}, a value ~ 10 times higher than Cu at room temperature.[5,6]

This excellent conductivity and charge carrier mobility of graphene suggests several applications in fast analog electronics, including transistors potentially operating in the THz regime, as well as graphene electrodes to replace ITO and graphene interconnects with low resistance and capacitance to replace copper. These applications do not require a high on–off ratio for switching, and thus are independent of the extensive efforts to create a band gap in graphene to enable its use for digital circuits.

The realization of any graphene-based device is dependent on finding functional substrates on which the high carrier mobility observed for freestanding sheets of graphene is maintained. A suspension geometry imposes significant constraints on device processing and creates serious reliability issues. To overcome these limitations, several materials have been tested as hosts of transferred graphene sheets, with the general conclusion that the mobility of charge carriers in freestanding graphene is degraded by bonding to a substrate, in some cases quite significantly. The majority of studies has focused on graphene transferred onto SiO_2, because of the desire for a high-quality, inexpensive dielectric substrate.[7] They produce mobility values in the range of 10^2–10^3 cm^2 V^{-1} s^{-1} at 300 K at a carrier concentration $n_G \sim 10^{12}$ cm^{-2}, a conductivity two to three orders of magnitude lower than for suspended graphene. Graphene transferred to h-BN substrates (very thin sheets of exfoliated BN) shows mobilities of $\sim 10^4$–10^5 cm^2 V^{-1} s^{-1} at 300 K and $\sim 10^5$ cm^2 V^{-1} s^{-1} at 10 K, at carrier concentrations $n_G \sim 10^{11}$–10^{12} cm^{-2}.[8] These mobilities appear to be the highest values so far achieved for supported graphene, but, of course, such substrates are also not ideal.

Factors limiting carrier mobility in substrate-supported graphene are currently

* Address correspondence to fcavallo@unm.edu and lagally@engr.wisc.edu.

Received for review June 22, 2014 and accepted September 9, 2014.

Published online September 09, 2014
10.1021/nn503381m

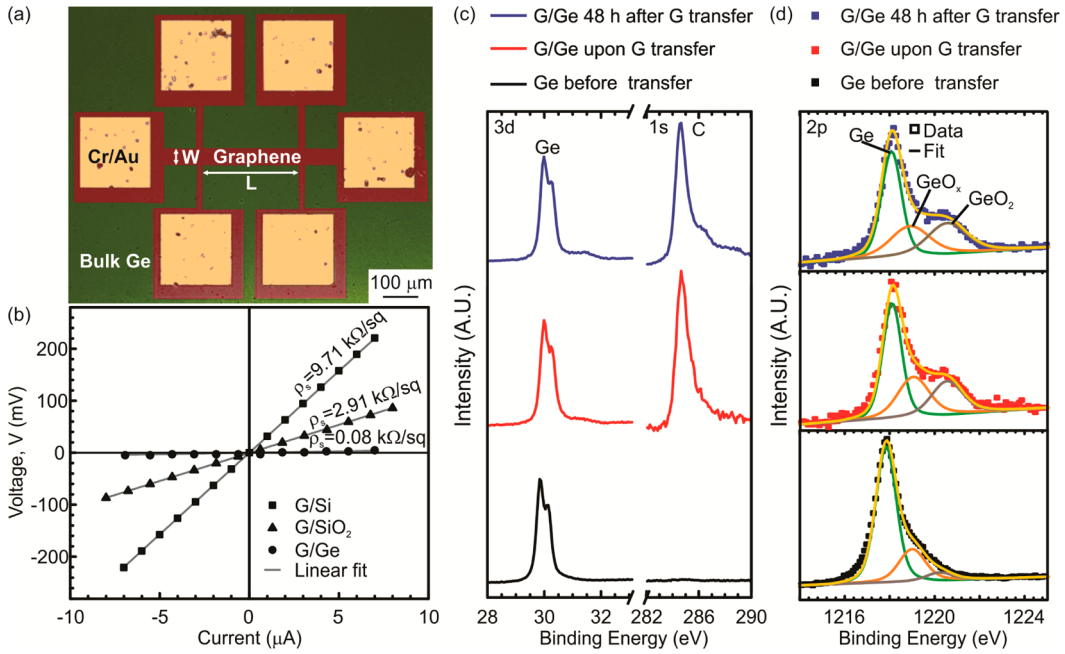

Figure 1. Resistance and X-ray photoelectron spectroscopy data for graphene transferred to several substrates. (a) False-color optical micrograph of a Hall bar fabricated in graphene transferred to a Ge(001) substrate. (b) Voltage–current characteristics measured for graphene transferred to H-terminated Si(001) (squares), SiO_2 (triangles), and Ge(001) (circles). Results are obtained from Hall bars having widths (W) of 85 μm and lengths (L) of 286 μm. The corresponding sheet resistivity values are shown. (c) Ge 3d and C 1s core-level spectra of Ge(001) before and after graphene transfer. The surface preparation of Ge before transfer of graphene (black curve) is described in the Materials and Methods. The red and blue curves are acquired immediately and 48 h after graphene transfer, respectively. The spectra are normalized to the Ge 3d peak amplitude; they are intended to show only the presence of graphene and the relative stability of the interfacial chemistry after graphene transfer. (d) Ge 2p core-level spectra corresponding to the three cases shown in (c). A stable GeO_x/GeO_2 layered structure is present at the graphene/Ge interface after transfer; before that only the suboxide is present. The V–I characteristic in (b) for graphene transferred to Ge(001) is obtained typically at a time between the red and blue curves in (c) and (d). The spectra are normalized to the Ge 2p peak amplitude.

under considerable debate.[1,9–13] Carrier scattering from charged impurities[14–21] trapped in the supporting substrate and at the graphene-substrate interface is thought to be significant. Host substrate roughness may result in rippling of the graphene sheet, which may also limit the charge carrier mobility.[1,4,22–24]

We report here exceptionally good charge transport properties for graphene transferred to a Ge(001) host. Charge transport in graphene supported on semiconductor substrates has not been extensively explored. Yet they are potentially good candidates to provide a high carrier mobility and a high conductivity in graphene because they are relatively smooth and can be highly resistive. The use of Si and Ge substrates for the fabrication of large-area devices can take advantage of well-established processing techniques. Additionally, Si and Ge are versatile host substrates, because the semiconductor behavior can be utilized in parts of a device that do not contain graphene. Finally, the surface structure and chemical behavior of these semiconductors are well-known.[25,26] As a result they can potentially be functionalized to achieve charge transfer between the substrate and graphene and thus tune carrier concentration to improve the conductivity in the graphene sheet.

RESULTS AND DISCUSSION

We investigated charge transport in graphene transferred to very lightly n-doped Ge(001) [nominal bulk dopant concentration $N_D \sim 6 \times 10^{13}$ cm^{-3}] with different surface conditions, and to H-terminated Si(001). In addition we studied transport in graphene transferred onto a SiO_2/bulk Si substrate as a reference system. Because of its unique properties, we focus here on the graphene/Ge(001) system, using the others as reference points. We used graphene grown by chemical vapor deposition (CVD) on Cu substrates; it allows growth of high-quality films over a large area and with high yield. We fabricated Hall bars in the transferred graphene, as reported in the Materials and Methods section. A typical device is shown in Figure 1(a).

Using these Hall bars, we made resistance measurements in a four-probe geometry at temperatures ranging from 10 to 300 K. Voltage–current characteristics acquired at 300 K are compared in Figure 1(b) for identical graphene Hall bars on three substrates, SiO_2, H-terminated Si(001), and Ge(001). The difference in slopes of these V–I curves confirms the strong influence of the supporting substrate on lateral charge transport in graphene. Specifically, V–I characteristics measured for graphene/SiO_2 and graphene/H-terminated Si(001) yield sheet resistivities of 2.91

and 9.71 kΩ/sq, respectively. The value of the resistivity for graphene on SiO_2 is similar to those previously reported,[1,4,27] confirming the reliability of our transfer technique and characterization methods. For graphene/Ge(001), on the other hand, the sheet resistivity is only ~0.08 kΩ/sq [Figure 1(b)]. We have repeated these results numerous times on different Hall bars and on different sheets of graphene transferred to Ge(001).

This low sheet resistivity is in and of itself of great interest, as it supports the use of graphene on Ge(001) in the applications of fast analog electronics mentioned earlier. The low resistivity may be due to a high carrier concentration or a high mobility. We consider both in turn.

As we believe that the graphene/Ge interface controls the electrical transport, we performed X-ray photoelectron spectroscopy (XPS) measurements of the Ge(001) substrate before and after graphene transfer. Figure 1(c) shows XPS spectra in the regions of the Ge 3d and C 1s peaks before (black curve) and after (red and blue curves) transfer of the graphene. Figure 1(d) shows the same spectra in the region of the Ge 2p peak, which, because of the lower kinetic energy of the emitted photoelectrons, is more sensitive to the near-surface region than the 3d peaks. Previous reports[28−31] show that a layered GeO_x/GeO_2 film forms on Ge(001). We therefore carefully analyzed the Ge 2p spectrum before, upon, and 48 h after graphene transfer to establish the existence of this GeO_x/GeO_2 film at the graphene-Ge interface. The spectra in Figure 1(d) are dominated by an elemental-Ge peak centered at ~1217 eV. Before graphene transfer a small shoulder is visible at higher binding energy. The shoulder can be attributed to a substoichiometric Ge oxide,[28−31] with a very small contribution from GeO_2 at somewhat higher binding energy. The spectra after graphene transfer (red and blue curves) show an immediate increase in the GeO_2 component, which grows only very slowly with time, while the GeO_x component remains more or less constant. The *V*−*I* characteristic shown in Figure 1(b) for graphene transferred to Ge(001) was measured within 48 h after the transfer.

With this information, we are able to suggest the possible origin of the low sheet resistivity measured in graphene/Ge(001). For that purpose we used a physical model based on traditional metal−semiconductor junction[32] theory and the unique energy structure of graphene.[1,33,34] We expect charge transfer to occur from Ge to graphene, leading to the graphene and the Ge surface to be populated with an excess of electrons and holes, respectively. Although an interface width of 3 nm (the combined oxide layers) is assumed in the calculations shown below, the resulting doping is quite insensitive to the barrier width, as may be expected. We calculate the type and concentration of carriers transferred to graphene using the band structures of n-doped Ge and of graphene reported in the

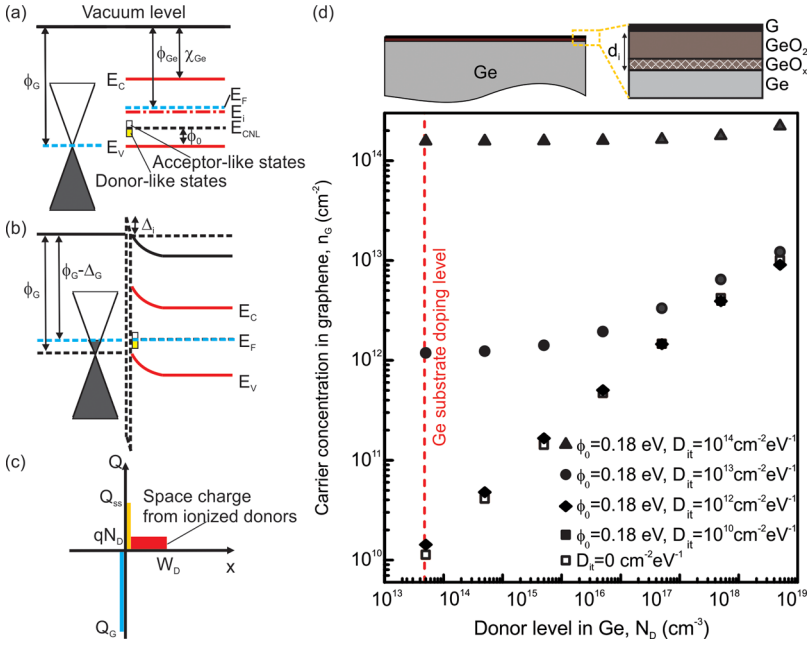

Figure 2. Electrical and structural model illustrating charge transfer across a graphene/oxidized-Ge junction. Schematic illustration of the band structure of graphene and oxidized, lightly doped Ge (a) before contact between the two materials occurs and (b) after a junction is formed and thermal equilibrium has been reached. A mixture of acceptor- and donor-like states is assumed, with the charge neutrality level, E_{CNL}, positioned 0.18 eV (ϕ_0) above the Ge valence band maximum. (c) Charge distribution in graphene and Ge as a result of charge transfer across the interface. (d) Calculated carrier concentration at 300 K in graphene *vs* doping level in an n-type Ge wafer. Above is a sketch of a cross-sectional view of graphene on oxidized Ge, detailing the multilayer structure at the graphene/substrate interface, including substoichiometric-Ge-oxide and GeO_2 layers. Calculations are performed at 300 K for several densities, D_{it}, of interface states. The red dashed line indicates the nominal doping level of the Ge(001) substrate used in our experiments. Values for D_{it} = 0 and D_{it} = 10^{10} cm^{-2} eV^{-1} give the same results.

literature.[32−34] In our analysis we take the effect of interface states into account. The model and results of the model are shown in Figure 2.

Figure 2(a) shows simplified band diagrams of graphene and lightly doped n-type Ge before the two materials come into contact. The graphene work function is taken to be the conventional literature value for undoped graphene, 4.5 eV,[33] greater than the work function of n-type Ge at any Ge bulk doping concentration considered here. From previous theoretical and experimental studies, the oxidized Ge surface, having a structure $Ge/GeO_x/GeO_2$, is known to have a mixture of acceptor- and donor-like trap states, with the charge neutrality level (CNL) (*i.e.*, the energy marking the point at which their densities are equal) located ∼0.18 eV above the valence band maximum of Ge.[35−37] A density of interface states, D_{it}, in the range of 10^{12}−10^{14} cm^{-2} eV^{-1} has been reported in the literature for $Ge/GeO_x/GeO_2$.[35−37] In Figure 2(b) we show the band diagrams of the graphene/Ge junction in thermal equilibrium after contact has occurred. Electrons have transferred from donor-like states at the G/Ge interface to graphene, leaving a positive surface charge (hole accumulation) behind. At the same time electrons residing in donor levels in the bulk of Ge lower their energy by occupying acceptor-like states at the Ge surface. Electrons transferred from bulk Ge to surface states leave behind an equal number of ionized donors in a region depleted of mobile carriers. Band-bending then occurs in Ge as the Fermi levels of graphene and Ge line up across the interface in proximity of the CNL (see Figure 2(b)).

Charge transfer between graphene and Ge has broken the symmetry of the electron and hole concentrations in the graphene, which is now electron doped. The Fermi level of graphene has risen from the Dirac points toward that of the Ge (n-type to a greater or lesser degree). Figure 2(c) schematically illustrates the charge distribution in graphene and Ge. A sheet of mobile electrons in graphene is counterbalanced by the positive charge associated with holes accumulated at the graphene/oxidized-Ge interface and by ionized donors in Ge.

Using the model illustrated in Figure 2(b) and (c), we calculated the density of charge carriers transferred to graphene bonded to an n-type Ge substrate that has a doping level N_D ranging from 5×10^{13} to 5×10^{19} cm^{-3}. We compare results obtained for ideal (D_{it} = 0 cm^{-2} eV^{-1}) and real graphene/oxidized-Ge junctions, with $D_{it} = \{10^{10}, 10^{12}, 10^{13}, 10^{14}\}$ cm^{-2} eV^{-1} at ϕ_0 = 0.18 eV, ϕ_0 being the difference between the energy of the CNL and the valence band maximum. Figure 2(d) plots the calculated carrier density in graphene *vs* doping concentration in Ge at room temperature for these cases. In an ideal graphene/oxidized-Ge junction, the amount of charge transferred to graphene from Ge increases monotonically with an increasing Ge bulk dopant concentration. This result is not surprising, as Ge substrates with a higher donor doping level have their Fermi energy farther from the graphene Fermi level when the two systems are not in contact [a greater work function difference]. Hence a higher Ge n doping results in a higher driving force for charge transfer across the graphene/Ge interface, but even at near degenerate doping levels in the Ge bulk, the carrier density in graphene is not exceptional without the presence of interface states.

When the density of interface states, D_{it}, is high, the effect on doping of graphene can be quite significant. At lower D_{it} the interface condition has a weaker influence on the charge transfer. Indeed, results for $D_{it} = 10^{10}$ cm^{-2} eV^{-1} are indistinguishable from those for D_{it} = 0. In contrast, as seen in Figure 2(d), in a graphene/oxidized-Ge junction with $D_{it} = 10^{14}$ cm^{-2} eV^{-1}, the concentration of carriers transferred to the graphene is very high and is only weakly dependent on the Ge substrate bulk dopant concentration.

We expect a D_{it} of the order of ∼10^{13} to 10^{14} cm^{-2} eV^{-1} for the graphene/oxidized-Ge interface.[35−37] The dashed vertical line in Figure 2(d) marks the concentration of donor dopants in the Ge substrates used in our experiments. Figure 2(d) shows that the values of carrier concentrations in graphene corresponding to the expected density, D_{it} ∼10^{13} to 10^{14} cm^{-2} eV^{-1}, of interface states lie between $n_G \sim 1.4 \times 10^{12}$ cm^{-2} and $n_G \sim 2 \times 10^{14}$ cm^{-2} at 300 K. The excess carriers in graphene are electrons. As stated earlier and shown in Figure 2(c), electrons in graphene are counterbalanced by holes accumulating on the Ge surface and the positive fixed charge of ionized donors. In the limit of high D_{it} the positive charge at the Ge surface is approximately balanced by the negative charge in graphene. This region enriched with mobile carriers at the Ge surface is separated from the bulk Ge by a depletion region. Specifically, the depletion width is of the order of several hundred micrometers for a D_{it} ∼10^{13}−10^{14} cm^{-2} eV^{-1} and the nominal bulk doping concentration $N_D \sim 6 \times 10^{13}$ cm^{-2} of the Ge substrate.

At this stage we have shown that transferring graphene to oxidized Ge(001) produces a very high conductivity in the graphene. We have proposed a model of the interface that arrives at a correspondingly high carrier concentration in the graphene, using only known values from the literature, *i.e.*, we have found a very efficient way to dope graphene, using charges from the Ge oxide interface. The uncertainties in the carrier concentration in graphene due to uncertainties in the input parameters are 1 order of magnitude.

Nevertheless, we now have to provide experimental proof of the high carrier density. For that purpose we performed Hall effect measurements. We show below that these provide carrier densities in reasonable agreement with those obtained by the model described in the previous paragraph. Using the Drude model,[32] we then extract the mobility of the charge

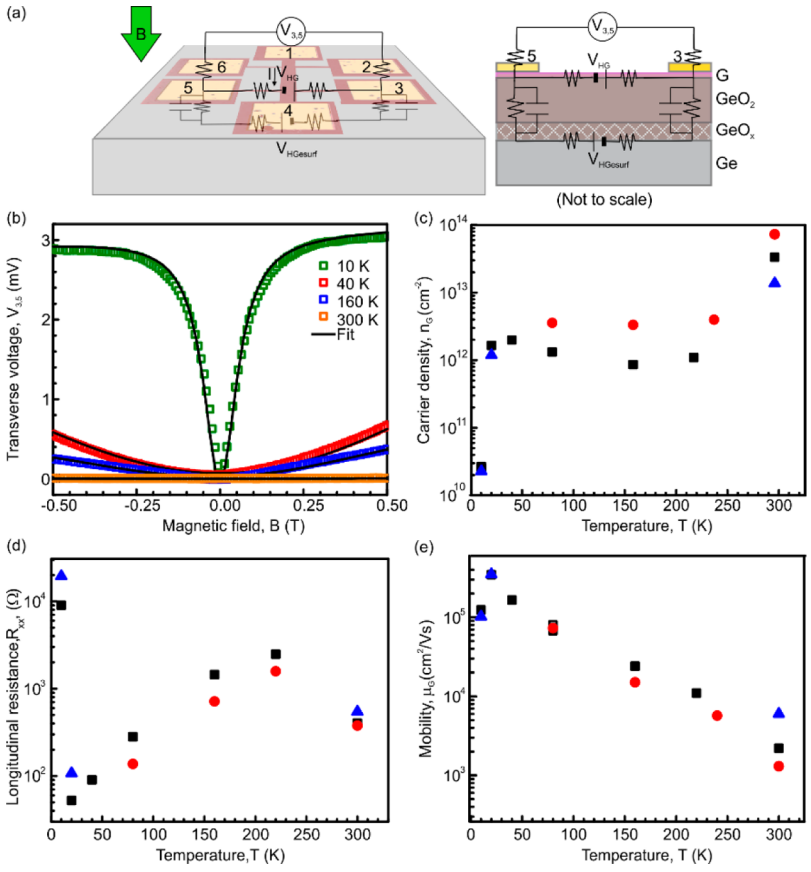

Figure 3. Charge transport measurements for graphene transferred to oxidized Ge(001). (a) Schematic three-dimensional and side views of the Hall bar structures and interfaces, along with equivalent circuits. The measurements were made at interface chemical conditions corresponding approximately to the middle XPS spectra in Figures 1(c) and (d). The heavy green arrow indicates the direction of the magnetic field corresponding to the circuit diagrams shown. (b) Typical dependence of the transverse voltage $V_{3,5}$ on magnetic field at different temperatures. (c) Temperature dependence of the carrier concentration in graphene/Ge(001), extracted by fitting $V_{3,5}$ *vs* B results from three Hall bars (different shapes and colors of symbols). (d) Longitudinal resistance, R_{xx}, of graphene transferred to oxidized Ge(001) measured as a function of temperature, for the same Hall bars. (e) Mobility as a function of temperature in graphene transferred to oxidized Ge(001), extracted from the data in (c) and (d). The three Hall bars are identical in dimensions but fabricated on different areas or on different sheets of transferred graphene. The uncertainties in repeated measurements on the same Hall bar are within the size of the data points, The one-order-of-magnitude sample-to-sample variation in n_G, R_{xx}, and μ_G reflects variations in the interface conditions, particularly D_{it}.

carriers in the graphene sheet. Our results demonstrate that the high mobility seen in free-suspended graphene sheets is maintained, or even exceeded, in this complex multi-interface system.

We evaluated the temperature dependence of charge transport by performing measurements of the longitudinal resistance, R_{xx}, at zero magnetic field, B = 0, and the transverse voltage, $V_{3,5}$, as the B field varies from −1 to 1 T. Results for B in the range of −0.5 to 0.5 T are shown in Figure 3. Specifically R_{xx} is obtained as $V_{2,3}/I_{1,4}$.The subscripts indicate the contact pads shown in Figure 3(a).

Figure 3(b) plots values of $V_{3,5}$ *vs* B acquired at different temperatures for one Hall bar. A nonlinear behavior is observed at all temperatures, with the "effective" Hall coefficient $R_H = V_{3,5}/I_{1,4}B$ decreasing with increasing temperature. This behavior may result when we have two conducting layers with different conductivity values and carrier types acting in parallel,[38−40] namely, the graphene layer, with electrons as carriers, and the Ge surface, with holes as carriers. The current $I_{1,4}$ forced through the Hall bar will split between the two conducting paths, in the graphene and in the Ge surface region. The Hall voltages arising within each layer will be different and opposite in sign. The existence of two carrier types will result in a potential difference across the interface between the graphene and the oxidized Ge, driving a current across the plane between them. This current produces voltage drops across the series resistances representing Ge and graphene, the interface impedences [across the plane between them], and the contact resistances. As a result the measured voltage $V_{3,5}$ does not directly reflect the internal Hall voltage in graphene.[38−40]

We model the graphene/GeO_2/GeO_x/Ge structure with the equivalent circuit shown in Figure 3(a).[38−40] We fit the data of Figure 3(b) by adjusting the resistances shown in Figure 3(a), and thereby extract the Hall voltage produced in graphene as a function of magnetic field. The fitting yields values of all circuit

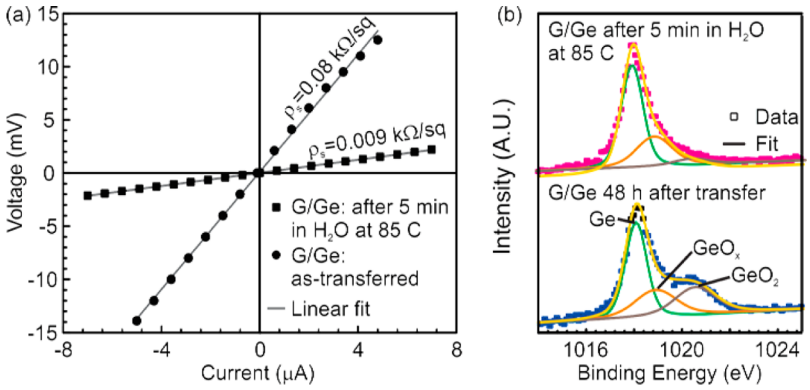

Figure 4. Effect of hot-deionized-water treatment on the resistivity of graphene transferred to Ge(001). (a) Voltage−current characteristics at 300 K using Hall bars with $W = 10\ \mu$m and $L = 286\ \mu$m before (solid circles) and after (solid squares) immersion in DI water at 85 °C for 5 min. The graphene-on-Ge(001) now shows a resistivity comparable to or lower than some metals.[25] (b) Ge 2p spectra for graphene/Ge(001) 48 h after initial transfer (bottom spectrum, same as top panel in Figure 1(d)) and immediately after immersion in DI water at 85 °C for 5 min (top spectrum). The GeO_2 has disappeared, while the GeO_x remains intact.

parameters shown in Figure 3(a), and reveals that the current in the graphene sheet is 2 orders of magnitude higher than the current in the underlying oxide/Ge interface region. The fit requires that interface impedences must have a component that depends on the sign of the *B* field.

The values of Hall voltage in the graphene, V_{HG}, so obtained are used to calculate carrier concentrations in graphene at temperatures from 10 to 300 K. Results are shown in Figure 3(c) for Hall bars fabricated on three different chips. The value of n_G stays effectively constant at 10^{12} cm^{-2}. At $T = 300$ K, the values of n_G are somewhat higher, of the order of $10^{13}-10^{14}$ cm^{-2}. We expect that at 300 K the activation of bulk-Ge dopants plays a role in determining n_G. The drop at very low temperatures may indicate a very slight activation energy for exciting interface states.

Measured values of longitudinal resistance for three devices are shown in Figure 3(d) as a function of temperature. The inferred values of carrier concentration in graphene, n_G, (Figure 3(c)), along with the measured values of longitudinal resistance, R_{xx} (Figure 3(d)) are used to calculate the carrier mobility, μ_G, according to[32]

$$\mu_G = \frac{L}{en_G R_{xx} W} \qquad (1)$$

The results, summarized in Figure 3(e), show a mobility from $>10^3$ to $\sim 5 \times 10^5$ cm^2 V^{-1} s^{-1} between 300 to 10 K. At temperatures below 80K, mobility values obtained *via* eq 1 using the data show in Figure 3 are comparable to or higher than ones at the same temperatures for suspended, edge-supported graphene or for graphene transferred and bonded to h-BN, the two systems with the highest reported mobilities. Comparison of the carrier concentrations in the graphene extracted from the Hall effect measurements (Figure 3(c)) and the values we predict with our graphene/oxidized-Ge interface model, using the density of Ge oxide interface states reported in the literature (Figure 2) shows quite reasonable agreement, given the number of parameters in the model and their interdependence. The mobility values quoted above would be even an order of magnitude higher if the carrier densities from Figure 2(c) are used in eq 1.

The high mobility is somewhat unexpected, because one might anticipate charge−charge scattering. We believe that the high mobility for graphene transferred onto oxidized Ge(001) is a consequence of a large density of fixed charges forming effectively a continuous sheet of charge at the graphene/Ge interface, yielding a constant or nearly constant electrostatic potential. As a result no or only weak localized potential fluctuations exist to scatter moving carriers. Furthermore, the absence of ripples in the graphene and a relatively smooth Ge surface (rms roughness ~0.3 nm) have been confirmed by atomic force microscopy (see Supporting Information). In this scenario we expect the dominant mechanism limiting carrier mobility to be in-plane acoustic and nonpolar optical-phonon scattering for a large portion of the investigated temperature range.[41] The trend shown in Figure 3(e) suggests that carrier mobility is limited by phonon scattering between 300 and 20 K, and that other scattering mechanisms prevail at lower temperatures.

The fact that the transport properties of graphene transferred to a host substrate are sensitive to the functionalization of the host surface,[42] as we indicated in the introduction, can be readily demonstrated for graphene on Ge(001). As indicated in the Materials and Methods, the final cleaning step of Ge(001) before transfer of graphene was immersion into deionized (DI) water at 85 °C for 5 min. When the combination of graphene/Ge(001) is immersed into DI water at the same conditions, the resistance drops below what is measured for the fully oxidized substrate. The *V*−*I* curve and XPS results are shown in Figure 4. XPS shows that this cleaning step dissolves the GeO_2 that had formed on the substrate surface during the graphene transfer,[29−31,43−46] but that the GeO_x layer remains intact. The dissolution occurs *via* attack at the

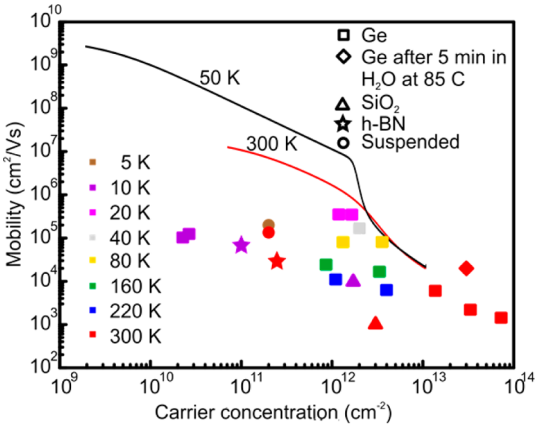

Figure 5. Comparison of the mobilities and charge carrier densities for various examples of transferred graphene, and for suspended graphene. (■) graphene/Ge(001), (▲) graphene/SiO_2,[48] (●) suspended graphene,[2,3] (★) graphene on a sheet or sandwiched between two sheets of h-BN,[8] (◆) DI-water treated graphene on Ge(001). Values obtained at different temperatures are shown as different colors. Graphene/Ge(001) results are uniformly higher than for other transfer systems. The uncertainties in the graphene-on-Ge values are approximately 1 order of magnitude.

edges of the Hall bar, and not through the graphene.[47] Using Hall effect measurements and analysis as above, we extracted a carrier concentration in the graphene at room temperature also of the order of $n_G \sim 10^{13}$ cm^{-2}. Using the measured conductivity (Figure 4(a)) in eq 1 then yields a mobility value of 2×10^4 cm^2 V^{-1} s^{-1} at room temperature. This topic will be discussed in more detail elsewhere.[47]

Finally we compare our results with other experimentally determined mobility values and with the theoretical limit of graphene mobility as a function of carrier concentration, as reported in ref 41. This comparison is shown in Figure 5. It is evident that the mobility values we measure at any temperature above 20 K combine with higher carrier densities than those of any other data. Furthermore, the carrier mobilities at 20 K (and 40 K within the margin of error) equal or exceed any other mobilities at any temperature (including those of suspended graphene) and do so at a higher carrier concentration. Above 20K, the mobilities we measure for graphene transferred to oxidized Ge(001) are near or at the theoretical limit.

CONCLUSIONS

We have demonstrated that the transfer of graphene to Ge(001), which provides a natural high density of interface states *via* its suboxide layer, creates a system in which the conductivity is very high, through both a high mobility and a high carrier concentration, even for an essentially insulating substrate. That this is possible on a semiconductor provides the added benefit that semiconductor functions and graphene functions can be readily combined on one platform. We can also conclude that thick Ge is not required, as long as the GeO_x interface is present. Thus, semiconductor nanomembranes (NMs)[49−51] can be used as substrates, opening the possibility of flexible and strain engineered semiconductor devices that also contain graphene as an element.

MATERIALS AND METHODS

Fabrication of Hall Bars in Graphene Transferred to a Host Substrate. A high-quality layer of graphene is grown on a Cu substrate by chemical vapor deposition (CVD). Next, a support layer, here poly(methyl methacrylate) (PMMA), is formed on the graphene *via* spin coating. The Cu growth substrate is then selectively removed from the structure by an iron chloride ($FeCl_3$) solution. After removal from the iron chloride solution, the graphene/PMMA combination is immersed in deionized (DI) water and then removed using the new host as the substrate. The result is a supported graphene film. After graphene transfer to the new host the PMMA support layer is finally selectively removed by a combination of acetone and isopropyl alcohol.

Hall bars patterns with varying widths and lengths are transferred to the supported graphene by optical lithography and oxygen plasma etching. A second lithography step and e-beam metal evaporation are used to deposit 5 nmCr/100 nmAu locally in the contact pad areas.

Substrate Surface Cleaning. In our experiments graphene was transferred to three different substrates, 300 nm thermally grown SiO_2 on Si(001), hydrogen terminated Si(001), and bulk Ge(001). Si(001) and Ge(001) are available commercially from many sources. Prior to the transfer of the graphene, the host substrates were cleaned as detailed below: (1) 5 min sonication in acetone followed by a 5 min sonication in isopropyl alcohol (IPA); (2) 10 s deionized (DI) water rinse at 25 C followed by N_2 blow drying; (3) 10 min UV ozone at 55 °C. Graphene was transferred directly to SiO_2. The Si(001) and Ge(001) substrates underwent additional cleaning steps. Si(001) was immersed in a 49% HF solution for 30 min followed by a DI water rinse. Ge(001) was immersed in DI water at 85 °C for 5 min. These treatments respectively remove the silicon dioxide and leave the Si(001) H terminated, and remove the stoichiometric GeO_2 from Ge(001). The suboxide is not soluble in water.

X-ray Photoelectron Spectroscopy. XPS analysis was performed using a Thermo Scientific K-Alpha instrument equipped with an Al Kα X-ray source that produces monochromatized radiation at 1486.6 eV. We used a 30 μm X-ray spot size and an analyzer pass energy of 20 eV, which, according to the manufacturer, provides an energy resolution of 0.57 eV. To obtain a better signal-to-noise ratio, 40 scans were averaged. The XPS spectra were fit with internal "Avantage" software. XPS data were collected on Ge before transfer of graphene, as soon after transfer as possible, and then periodically after that.

Electrical-transport and XPS measurements were made on different samples prepared identically. In order to match surface/interface conditions of the graphene/Ge combination at the time after transfer at which the electrical measurements were made, the sample was left in air and reintroduced into the XPS chamber every day for analysis. Subsequently the XPS spectra were matched in time to the time of electrical measurements.

Only the positions of peaks and their relative magnitudes were used in drawing the conclusion in this paper; no effort was made at quantitative concentration analysis and none is needed to reach the conclusions of this paper.

Electrical Characterization. Ge(001) wafers were acquired from Wafer World, Inc. They are 500−550 μm thick with a resistivity >40 Ω-cm. Using the specifications given by the vendor and the

room temperature electron mobility of Ge, this resistivity equates to a carrier concentration of $<4 \times 10^{13}$ cm^{-3}. To confirm the vendor's resistivity specification, van der Pauw measurements were made on an 8×8 mm^2 piece of Ge at room temperature in order to obtain the sheet resistance. This value was then used to calculate the Ge resistivity for the wafer thickness provided by the vendor. The extracted resistivity of 50−55 Ω-cm (close to that provided) gives a charge carrier concentration in our Ge wafers of $\leq 6 \times 10^{13}$ cm^{-3}.

Current−voltage characteristics were acquired by a four-probe technique using a probe station equipped with a semiconductor parameter analyzer (Agilent 4156C, input impedance $\geq 10^{15}$ Ω, current set resolution 1 nA, and voltage measurement resolution 2 μV). For four-probe measurements (see Figure 3), a current is passed between probes 1 and 4 and the resulting voltage drop is measured across probes 2 and 3.

The carrier sign and carrier concentration measurements use a standard Hall effect technique. A physical property measurement system (PPMS) (Quantum Design Model 6000) and a lock-in amplifier (Signal Recovery 7265 DSP) are used. For Hall effect measurements, an AC current at a frequency 37 Hz is passed between contacts 1 and 4 and the Hall voltage is measured across contacts 3 and 5 (Figure 3) in the presence of a magnetic field swept between ±3 T at a rate of 0.01 T. The current is typically swept over ±1 μA at each magnetic field. In the graphs in Figure 3, the offset voltage measured at $B = 0$ was subtracted from the data sets.

For the samples represented by square and circle data points in Figure 3(c−e), temperature dependence experiments were done by cooling the sample at a rate of 2 K per min. After the desired lowest temperature was reached (10 K), the sample was allowed to stabilize before beginning Hall effect measurements. After completing these measurements, the temperature was increased at a rate of 2 K per min to the next higher temperature at which Hall effect measurements were performed. For the sample represented by triangle data points, the temperature dependence measurements were performed in the reverse direction, starting at room temperature until 10 K was reached.

Modeling. Wolfram Mathematica 5.0 was used to calculate the results reported in Figure 2(c). Semianalytical modeling of the Hall effect measurements (Figure 3(b)) was performed combining circuit analysis and a fitting procedure to calculate circuit parameters. For this purpose we used Wolfram Mathematica 5.0 and OriginPro 8.5.

Conflict of Interest: The authors declare the following competing financial interest(s): R.R.D., F.C., and M.G.L. have filed a patent application related to the graphene/Ge system.

Acknowledgment. This work was supported by DOE, Grant No DE-FG02-03ER46028. The fabrication of graphene at Notre Dame was supported in part by ND Nano Center, by the NRI MIND Center, and by NSF (H.X. CAREER award). M.K. and H.X. fabricated the graphene; R.R.D., J.S.P., and D.P.S. fabricated the samples and made measurements; F.C., R.R.D., M.A.E., and M.G.L. analyzed and/or modeled the data; F.C., R.R.D., and M.G.L. wrote the paper. The authors thank F. Liu, M. S. Arnold, R. Jacobberger, I. Knezevic, N. Sule, F. S. Flack, D. E. Savage, and S. A. Scott for stimulating discussions.

Supporting Information Available: Atomic force microscope image of a Ge(001) substrate. This material is available free of charge *via* the Internet at http://pubs.acs.org.

REFERENCES AND NOTES

1. Neto, A. H.; Guinea, F.; Peres, N. M. R.; Novoselov, K. S.; Geim, A. K. The Electronic Properties of Graphene. *Rev. Mod. Phys.* **2009**, *81*, 109–162.
2. Bolotin, K.; Sikes, K. J.; Jiang, Z.; Klima, M.; Fundenberg, G.; Hone, J.; Kim, P.; Störmer, H. L. Ultrahigh Electron Mobility in Suspended Graphene. *Solid State Commun.* **2008**, *146*, 351–355.
3. Bolotin, K.; Sikes, K. J.; Störmer, H. L.; Hone, J.; Kim, P. Temperature-Dependent Transport in Suspended Graphene. *Phys. Rev. Lett.* **2008**, *101*, 096802.
4. *CRC Materials Science and Engineering Handbook*; Shackelford, J. F., Alexander, W., Eds.; CRC Press: Boca Raton, FL, 2000; p 941.
5. Trushin, M.; Schliemann, J. Minimum Electrical and Thermal Conductivity of Graphene: A Quasiclassical Approach. *Phys. Rev. Lett.* **2007**, *99*, 216602.
6. *CRC Materials Science and Engineering Handbook*; Shackelford, J. F., Alexander, W., Eds.; CRC Press: Boca Raton, FL, 2000; p 384.
7. Dorgan, V. E.; Bae, M.-H.; Pop, E. Mobility and Saturation Velocity in Graphene on SiO_2. *Appl. Phys. Lett.* **2010**, *97*, 082112.
8. Dean, C. R.; Young, A. F.; Meric, I.; Lee, C.; Wang, L.; Sorgenfrei, S.; Watanabe, K.; Taniguchi, T.; Kim, P.; Shepard, K. L.; Hone, J. Boron Nitride Substrates for High-Quality Graphene Electronics. *Nat. Nanotechnol.* **2010**, *5*, 722–726.
9. Schedin, F.; Geim, A. K.; Morozov, S. V.; Hill, E. W.; Blake, P.; Katsnelson, M. I.; Novoselov, K. S. Detection of Individual Gas Molecules Adsorbed on Graphene. *Nat. Mater.* **2007**, *6*, 652–655.
10. Adam, S.; Hwang, E. H.; Galitski, V. M.; Das Sarma, S. A Self-Consistent Theory for Graphene Transport. *Proc. Natl. Acad. Sci. U. S. A.* **2007**, *104*, 18392–18397.
11. Stauber, T.; Peres, N. M. R.; Guinea, F. Electronic Transport in Graphene: A Semiclassical Approach Including Midgap States. *Phys. Rev. B: Condens. Matter Mater. Phys.* **2007**, *76*, 205423.
12. Katsnelson, M. I.; Geim, A. K. Electron Scattering on Microscopic Corrugations in Graphene. *Philos. Trans. R. Soc., A* **2008**, *366*, 195–204.
13. Tan, Y. W.; Zhang, Y.; Bolotin, K.; Zhao, Y.; Adam, S.; Hwang, E. H.; Das Sarma, S.; Störmer, H. L.; Kim, P. Measurement of Scattering Rate and Minimum Conductivity in Graphene. *Phys. Rev. Lett.* **2007**, *99*, 246803.
14. Chen, J. H.; Jang, C.; Adam, S.; Fuhrer, M. S.; Williams, E. D.; Ishigami, M. Charged-Impurity Scattering in Graphene. *Nat. Phys.* **2008**, *4*, 377–381.
15. Yan, X.-Z.; Romiah, Y.; Ting, C. S. Electric Transport Theory of Dirac Fermions in Graphene. *Phys. Rev. B: Condens. Matter Mater. Phys.* **2008**, *77*, 125409.
16. Novikov, D. S. Numbers of Donors and Acceptors from Transport Measurements in Graphene. *Appl. Phys. Lett.* **2007**, *91*, 102102.
17. Adam, S.; Hwang, E. H.; Das Sarma, S. Scattering Mechanisms and Boltzmann Transport in Graphene. *Phys. E* **2008**, *40*, 1022–1025.
18. Hwang, E. H.; Adam, S. Das Sarma, Carrier Transport in Two-Dimensional Graphene Layers. *Phys. Rev. Lett.* **2007**, *98*, 186806.
19. Cheianov, V. V.; Fal'ko, V. I. Friedel Oscillations, Impurity Scattering, and Temperature Dependence of Resistivity in Graphene. *Phys. Rev. Lett.* **2006**, *97*, 226801.
20. Nomura, K.; MacDonald, A. H. Quantum Transport of Massless Dirac Fermions. *Phys. Rev. Lett.* **2007**, *98*, 076602.
21. Ando, T. Screening Effect and Impurity Scattering in Monolayer Graphene. *J. Phys. Soc. Jpn.* **2006**, *75*, 074716.
22. Ishigami, M.; Chen, J. H.; Cullen, W. G.; Fuhrer, M. S.; Williams, E. D. Atomic Structure of Graphene on SiO_2. *Nano Lett.* **2007**, *7*, 1643–1648.
23. Morozov, S. V.; Novoselov, K. S.; Katsnelson, M. I.; Schedin, F.; Elias, D. C.; Jaszczak, J. A.; Geim, A. K. Giant Intrinsic Carrier Mobilities in Graphene and its Bilayer. *Phys. Rev. Lett.* **2008**, *100*, 016602.
24. Teng, L.; Zhao, Z. Substrate-Regulated Morphology of Graphene. *J. Phys. D: Appl. Phys.* **2010**, *43*, 075303.
25. Kingston, R. H. Review of Germanium Surface Phenomena. *J. Appl. Phys.* **1956**, *27*, 101–114.
26. Dabrowski, J. and Muessig, H.-J. *Silicon Surfaces and Formation of Interfaces: Basic Science in the Industrial World*; World Scientific Pub. Co.: Singapore, 2000.
27. Cooper, D. R.; D'Anjou, B.; Ghattamaneni, N.; Harack, B.; Hilke, M.; Horth, A.; Majlis, N.; Massicotte, M.; Vandsburger, L.; Whiteway, E.; Yu, V. Experimental Review of Graphene. *ISRN Condens. Matter Phys.* **2012**, 501686.
28. Schmeisser, D. Surface Oxidation States of Germanium. *Surf. Sci.* **1986**, *172*, 455–465.
29. Bodlaki, D.; Yamamoto, H.; Waldeck, D. H.; Borguet, E. Ambient Stability of Chemically Passivated Germanium Interfaces. *Surf. Sci.* **2003**, *543*, 63–74.

30. Park, K.; Lee, Y.; Lee, J.; Lim, S. Oxidation Mechanism of Hydrogen-Terminated Ge(100) Surface. *Appl. Surf. Sci.* **2008**, *254*, 4828–4832.
31. Kuzum, D.; Krishnamohan, T.; Pethe, A. J.; Okyay, A. Y.; Oshima, Y.; Sun, Y.; McVittie, J. P.; Pianetta, P. A.; McIntyre, P. C.; Saraswat, K. C. Ge Interface Engineering with Ozone Oxidation for Low Interface State Density. *IEEE Electron Device Lett.* **2008**, *29*, 328–330.
32. Sze, S. M.; Ng, K. K.; *Physics of Semiconductor Devices*; Wiley: New York, 1981.
33. An, Y.; Benham, A.; Pop, E.; Ural, A. Metal-Semiconductor-Metal Photodetectors Based on Graphene/p-type Silicon Schottky Junctions. *Appl. Phys. Lett.* **2013**, *102*, 013110.
34. Zhong, H.; Xu, K.; Liu, Z.; Xu, G.; Shi, L.; Fan, Y.; Wang, J.; Ren, G.; Yang, H. Charge Transport Mechanisms of Graphene/Semiconductor Schottky Barriers: A Theoretical and Experimental Study. *J. Appl. Phys.* **2014**, *115*, 013701.
35. Kuzum, D.; Martens, K.; Krishnamohan, T.; Saraswat, K. C. Characteristics of Surface States and Charge Neutrality Level in Ge. *Appl. Phys. Lett.* **2009**, *95*, 252101.
36. Grassman, T. J.; Bishop, S. R.; Kummel, A. C. An Atomic View of Fermi Level Pinning of Ge(100) by O_2. *Surf. Sci.* **2008**, *602*, 2373–2381.
37. Hashemi, F.; Thombare, S.; Fontcuberta i Morral, A.; Brongersma, M. L.; McIntyre, P. C. Effects of Surface Oxide Formation on Germanium Nanowire Band-edge Photoluminescence. *Appl. Phys. Lett.* **2013**, *102*, 251122.
38. Hurd, C. M.; McAlister, S. P.; McKinnon, W. R.; Stewart, B. R.; Day, D. J.; Mandeville, P.; SpringThorpe, A. J. Modeling Parallel Conduction in GaAs/Al_xGa_{1-x}As Heterostructures. *J. Appl. Phys.* **1988**, *63*, 4706.
39. Look, D. C.; Stutz, C. E.; Bozada, C. A. Analytical Two-Layer Hall Analysis: Application to Modulation-doped Field-Effect Transistors. *J. Appl. Phys.* **1993**, *74*, 311–315.
40. Arnaudov, B.; Paskova, T.; Evtimova, S.; Valcheva, E.; Heuken, M.; Monemar, B. Multilayer Model for Hall Effect Data Analysis of Semiconductor Structures with Step-Changed Conductivity. *Phys. Rev. B: Condens. Matter Mater. Phys.* **2003**, *67*, 045314.
41. Sule, N.; Knezevic, I. Phonon-Limited Electron Mobility in Graphene Calculated Using Tight-Binding Bloch Waves. *J. Appl. Phys.* **2012**, *112*, 053702.
42. Baltazar, J.; Sojoudi, H.; Paniagua, S. A.; Kowalik, J.; Marder, S. R.; Tolbert, L. M.; Graham, S.; Henderson, C. L. Facile Formation of Graphene P−N Junctions Using Self-Assembled Monolayers. *J. Phys. Chem. C* **2012**, *116*, 19095–19103.
43. Kim, J.; McVittie, J.; Saraswat, K. C.; Nishi, Y.; Liu, S.; Tan, S. Germanium Surface Cleaning with Hydrochloric Acid. *ECS Trans.* **2006**, *3*, 1191–1196.
44. Chan, L. H.; Altman, E. I.; Liang, Y. Development of Procedures for Obtaining Clean, Low-Defect-Density Ge(100) Surfaces. *J. Vac. Sci. Technol., A* **2001**, *19*, 976–982.
45. Hovis, J. S.; Hamers, R. J.; Greenlief, C. M. Preparation of Clean and Atomically Flat Germanium (001) Surfaces. *Surf. Sci.* **1999**, *440*, L815–L819.
46. Oh, J.; Campbell, J. E. Thermal Desorption of Ge Native Oxides and the Loss of Ge from the Surface. *J. Electron. Mater.* **2004**, *33*, 364–367.
47. Rojas Delgado, R.; Cavallo, F.; Lagally, M. G. Kinetics of Ge oxidation in graphene/Ge, unpublished.
48. Novoselov, K. S.; Geim, A. K.; Morozov, S. V.; Jiang, D.; Zhang, Y.; Dubonos, S. V.; Grigorieva, I. V.; Firsov, A. A. Electric Field Effect in Atomically Thin Carbon Films. *Science* **2004**, *306*, 666–669.
49. Cavallo, F.; Lagally, M. G. Semiconductors Turn Soft: Inorganic Nanomembranes. *Soft Matter* **2010**, *6*, 439–455.
50. Scott, S. A.; Lagally, M. G. Elastically Strain-Sharing Nanomembranes: Flexible and Transferable Strained Silicon and Silicon−Germanium Alloys. *J. Phys. D: Appl. Phys.* **2007**, *40*, R75–R92.
51. Rogers, J. A.; Lagally, M. G.; Nuzzo, R. G. Semiconductor Nanomembranes: Synthesis, Assembly, and Applications. *Nature* **2011**, *477*, 45–54.